2026 IEEE International Conference on Robotics and Automation (ICRA 2026)
June 1-5, 2026. Vienna, Austria

Gravity-Assisted Shape-Locking Articulated Discrete Serial Robot for Ceiling-Mounted Manipulation in Patient Care

Seonhun Lee[1] and Frank C. Sup IV[1]

Abstract— **Continuum robots are promising for assistive manipulation, but often lack the stiffness and payload capacity required for real-world tasks. This paper investigates the feasibility of a novel dual-mode, gravity-assisted ceiling-mounted articulated discrete serial robot that transitions between passive and active states using a friction-based shape-locking mechanism. In passive mode, joints are unlocked, allowing for chain-like flexibility similar to that of ceiling hoists. In active mode, joints are locked, allowing for rigid and accurate manipulation. To evaluate feasibility, we implemented a reduced-scale prototype with two passive joints and one active joint. We tracked its accuracy across 300 iterations of point-to-point motion in a 2D plane. Results show high repeatability and robustness, highlighting the potential of this architecture for ceiling-mounted manipulation. Beyond healthcare tasks such as patient handling, this approach contributes a scalable actuation and shape-locking strategy for articulated discrete serial robots in constrained environments.**

I. Introduction

To address rising nursing workloads that strain staff and impact care quality, hospitals are turning to robotic technologies [1], [2]. The broader healthcare robotics market is expanding rapidly, with forecasts projecting sustained double-digit growth through 2030 [3]. Much of this development has concentrated on logistics, telepresence, or surgical systems, but far fewer efforts target robots that can directly support patient care and the daily workflow of nurses. This integration of robots is generally viewed positively by nurses, who see them as assistive tools that enhance care quality and allow nurses to dedicate more time to patient interactions [2], [4].

Direct patient-handling tasks, such as lifting and repositioning, are some of the physically demanding activities in nursing, reporting 12% of nurses leaving the occupation due to back pain from patient handling in 2011 [5]. Ceiling lifts are widely deployed to reduce physical strain, but these systems are rigid and limited to vertical hoisting. Mobile assistive robots have been explored; however, crowded patient rooms raise concerns about safety and workflow. Bernad et.al. [6] warn of the risks of robots interacting with patients and the staff surrounding a robot. The paper addresses a small error margin in path planning and object avoidance that a robot needs to perform to ensure safety. A ceiling-mounted robotic approach offers the potential to extend existing infrastructure with more adaptable interaction while avoiding floor-space conflicts. Although highly beneficial, ceiling lifts have their own limitations.

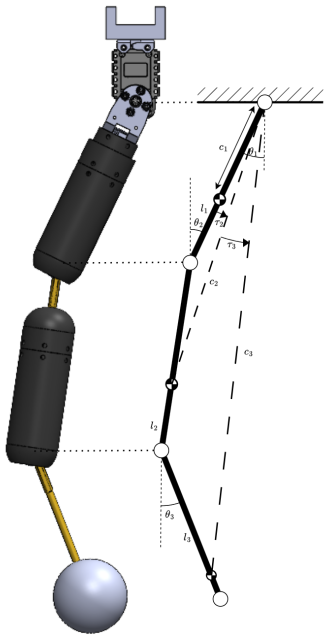

Fig. 1. Concept of the evaluation setup of one active and two passive joint ceiling robot arm.

Ceiling lifts typically consist of a rope or sling with a handle attachment that descends from a winch system, which travels along a rail or gantry system. Gantry-based ceiling systems have been widely adopted for patient lifting tasks due to their ability to support substantial loads through gravity-aligned suspension. [7], [8] However, these systems often have limitations in dynamic environments, particularly when the lifting rope becomes unloaded or slack. This results in uncontrolled oscillations in both lateral and torsional stability. [9] While passive rope structures are mechanically advantageous for bearing heavy loads, their lack of configurability limits controllability.

As a solution, this paper proposes a modular chain mechanism for an articulated discrete serial-based ceiling robot that utilizes an embedded locking mechanism to maintain its shape, as shown in Figure 1. The design modulates the stiffness and geometry under low-load conditions, improving stability beyond passive rope systems. Active manipulation capabilities further enable precise repositioning of the end-effector, making ceiling-mounted interaction more versatile.

This research investigates a dual-mode, compact, gravity-

Generative AI tools(Grammarly) were solely used exclusively for grammar refinement and clarity improvements.

[1]This work was supported by Elaine Marieb Center for Nursing and Engineering Innovation.

[1]Department of Mechanical and Industrial Engineering, University of Massachusetts Amherst, Amherst, MA 01003 USA.
Email: seonhunlee@umass.edu, sup@umass.edu

assisted articulated discrete serial robot designed to support patient care tasks, including procedure preparation, assistance, and cleanup. We demonstrate feasibility through a reduced-scale prototype. In passive mode, the robot behaves as a chain-like structure, and in active mode, its joints are friction-locked to maintain the desired configurations. The prototype validates the mechanics and performance of this dual-mode architecture.

II. Background

A. Shape-Locking Mechanisms

Continuum robots are regarded as promising tools for healthcare applications, where human safety, flexibility, and gentle interaction are essential [10]. However, their inherent flexibility poses significant challenges in hospital settings. Continuum arms frequently encounter issues with low stiffness, significant twisting, and buckling when subjected to load, potentially affecting their accuracy, payload capacity, and overall dependability [11], [12].

These robots have been focusing on improving load-bearing capabilities by implementing various techniques. The most versatile method for achieving this is through a variable stiffness approach. This can be achieved by using transition elements, such as shape memory alloys(SMA) [13], magnetorheological fluids [14], magnet [15], or flexible fluidic actuators such as McKibbin actuators [16]. Rather than making material changes, stiffness can be varied using the cross-section shaping method [17], [18]. Multi-material composites, such as multi-layer jamming [19] and multi-layer beaming [20], have also been explored. Among the most common jamming and locking methods, such as a layer [21], wire [22], or granular [23], were considered most effective with a fast reversible process [24]. A review by Blanc et al. compares the efficacy of these various shape-locking methods [25]. To achieve the stable fixation of the shape in place, high stiffness is required. According to Blank, out of these various techniques, there are only three methods that can actually lock the joints: Low Melting Point Alloy (LMPA), SMA, and mechanical solutions.

Contrary to mechanical solutions, both LMPA and SMA [26] based solutions are intrinsically slow in activation and deactivation due to the requirements of thermal energy for activation. The LMPA-based soft robot presented by McCabe [27] required approximately 240 seconds to heat a single joint and roughly 100 seconds to cool down. To keep the actuation in a feasible time frame, a mechanical solution is considered most optimal.

B. Gravity Assisted Robots

In 1990, McGeer presented a classic walking robot using solely gravity on a slope [28]. From then on, few robots were designed to utilize gravity as an actuation system. When designing a robotic system, gravity is typically viewed as an obstacle that must be overcome [29], [30]. This is due to motors being required to use excessive energy solely on compensating gravitational torque from the masses [31]. This is also the case in a continuum robot. However, gravity is a consistent and reliable force that can be advantageous for ceiling robots. The motion is generally aligned with the direction of gravity. Thus, the use of gravity as an actuation mechanism for a ceiling robot warrants an investigation.

III. Design Overview

A. Design Concept

To meet the functional requirements of nursing-assistive robotics, including patient handling and spatial working area, a retractable, articulated, discrete serial robot arm is proposed. This arm operates in two modes: load-bearing capacity for both passive and active use. In passive mode, the locking mechanism is disengaged, allowing the joints to articulate freely. This is achieved through a joint architecture analogous to unconstrained ball-and-socket configurations, permitting multi-directional movement without resistance. Functionally, the articulated discrete serial arm in this state resembles the chain mechanism of ceiling-mounted hoists commonly found in hospital settings. The final goal for the ceiling robot arm is designed to be drawn and extruded from a spool, facilitating compact storage and rapid deployment. During passive operation, vertical motion is mechanically constrained, and the load-bearing capacity is determined solely by the tensile and compressive strength of the constituent materials.

In active mode, the system transitions into a structurally rigid configuration. Each joint can be selectively locked using friction jamming techniques, allowing the arm to maintain a fixed shape under load. The robot arm comprises two primary subsystems: a passive joint/link segment and an active actuation module. The active module governs the extrusion and angular positioning of subsequent joints, which are then locked into place once the desired orientation is achieved.

The locking of passive segments occurs once the target angle is reached. As the active segment rotates, it drives the motion of the following link, which settles into position under the influence of gravity. This gravitational settling ensures that each joint aligns with its center of mass, contributing to the overall stability of the structure.

While in passive mode, the joints of the robot arm are unlocked, allowing each joint to move freely, similar to chain linkages. This functionality is comparable to the ceiling lifts currently used in hospitals. Although the robot arm cannot bend its linkages to reposition the payload in passive mode, its functionality is expected to be similar to existing solutions.

The shape-locking mechanism allows the robot arm to maintain its desired position. Figure 2 illustrates the internal structure and mechanism of a friction-based shape-locking system utilizing a lead screw. A small N20 motor with a gearbox (6V, 30 RPM, 1:100) for torque multiplication rotates a lead screw, whose lead nut is attached to a braking block, which applies a linear force to the ball joint.

Because the system relies on friction braking, a braking force is needed to withstand both the payload and the weight of the subsequent joints. Thus, the braking force should be

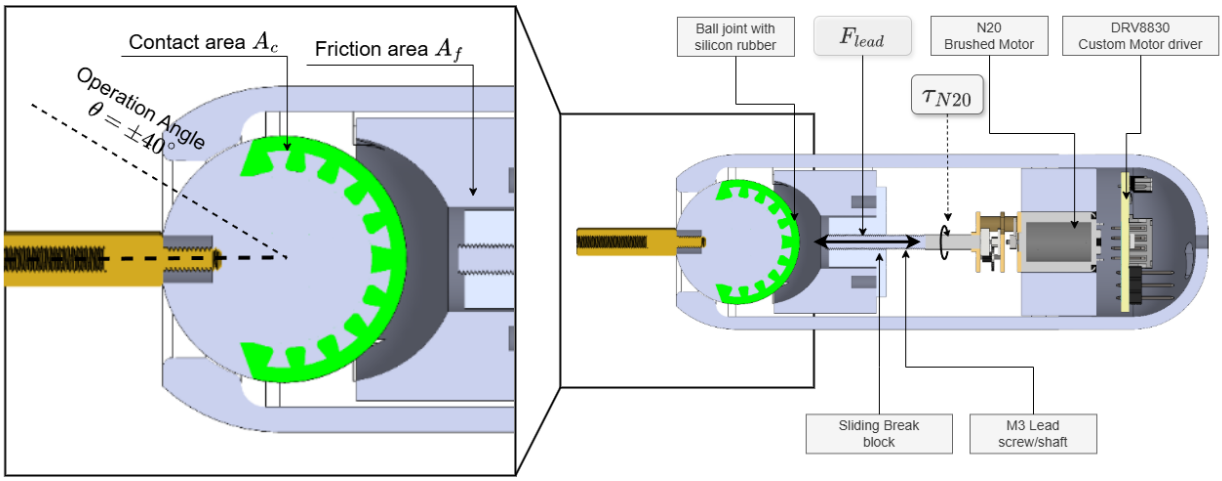

Fig. 2. Free-body diagram of force transfer shape-locking mechanism and internal components of linkages and mechanism for shape-locking.

greater than the whole payload. Since the motor and the lead screw introduce the braking force, the necessary friction force can be calculated as

$$\begin{aligned} \sum_{i=0}^{n} m_n g \leq F_f &= \mu F_N \\ &= \mu P \left(A_c + A_f\right) \\ &= \mu \frac{F_{linear}}{A_f} \left(A_c + A_f\right) \end{aligned} \tag{1}$$

Here A_f and A_c are the friction pad area and contact area, respectively.

Since the motor drives the lead screw, the force it generates is as follows.

$$F_{linear} = \frac{2\pi\eta K_t I}{l_{lead}} \quad \begin{cases} F & = \frac{2\pi\eta}{l}\tau_{motor} \\ \tau_{motor} & = K_t \tau_{stall} = K_t I \end{cases} \tag{2}$$

here l_{lead} denotes the length of lead screw.

B. Shape-Locking Mechanism

Although there are many shape-locking methods, we have chosen the simplest friction-locking method, utilizing motor force, to test the validity of the system. The central computer sends a signal to the I2C addressable DRV8830 motor driver, which in turn drives the internal N20 brushed motor through a gearbox that reduces the RPM. The attached lead screw and shaft move the braking block. The block engages with a ball joint featuring a half-section made of silicon rubber to increase the friction coefficient. This is achieved by silicon molding with a thin contact layer, ensuring that the torsional stiffness remains high and therefore negligible.

Ball joints are designed to facilitate unrestricted rotations, allowing for continuous articulation. These joints operate with a rotational constraint of ± 40 degrees, enabling flexibility while maintaining stability. To increase the friction coefficient and improve performance, one half of each ball joint is filled with high-viscosity silicone, which provides added resistance and dampening effects. This design choice not only increases the joint's overall durability but also increases the friction force, allowing the joint to withstand varying loads.

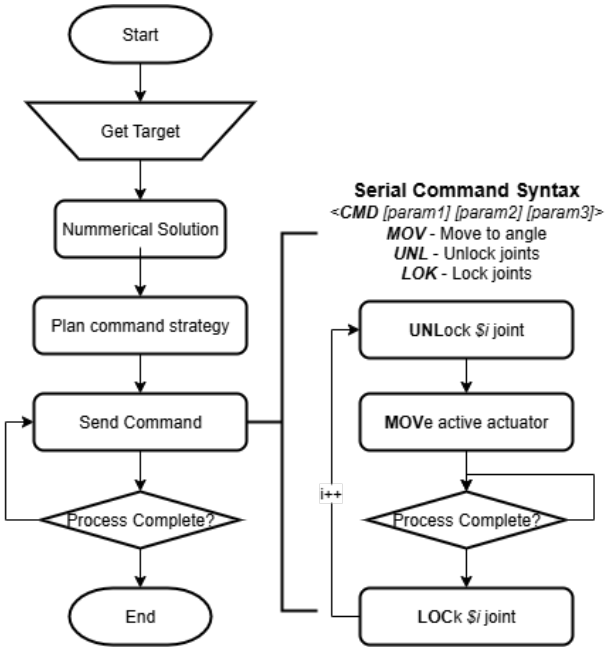

Fig. 3. Control system flow from user input to command strategy formulation.

IV. Control Scheme

To initiate motion planning, a desired end-effector position is first defined within the robot's workspace. Inverse kinematics are then computed using an iterative numerical solver. The numerical solver explores the solution space through optimization techniques. This is further explained in *Inverse Kinematics* subsection. Once the optimal joint-space configuration is determined, a corresponding command sequence is generated. The microcontroller then executes the planned commands through the motor controller. The process is depicted in Figure 3. Command strategy is formulated by stacking *unlock joint*, *move active actuator*, and *lock joint*. This is controlled by using Arduino MKR1000 with Dynamixel Shield from Robotis.

A. Inverse Kinematics

Let the position of the end-effector be $\mathbf{p}_3 = [x_3, y_3, z_3]^T$. Each link vector $\vec{v}_i$ is defined in spherical coordinates as:

$$\vec{v}_i = l_i \begin{bmatrix} \sin(\theta_i)\cos(\phi_i) \\ \sin(\theta_i)\sin(\phi_i) \\ -\cos(\theta_i) \end{bmatrix} \tag{3}$$

The total position of the end-effector is the sum of the subsequent vectors:

$$\vec{p}_k = \sum_{i=1}^{k} \vec{v}_i \tag{4}$$

When the bending amount is equally weighted, the arms tend to curve at an equal angle, thus making a soft arc. This results in deviation of the center of mass from the direct center. This is expected to increase the necessity for more substantial torque, thus reducing the efficiency of the system. Therefore, to set a rough estimate of the desired shapes of the solution, a weight bias system was implemented. Each weight, a value between 0 and 1, can define the amount of deflection each joint will apply.

$$\vec{p}_k = \sum_{i=0}^{k} \vec{v}_i w_i PE_i \tag{5}$$

here p_d denotes the desired location, w_i for weights, and PE_i for potential energy at the state. With this, a solution can be found iteratively using the error.

$$\begin{aligned} 0\text{minimize} \quad & \|\vec{p}_k - \vec{p}_d\| \\ \text{subject to} \quad & \theta_1 \in [-\pi, \pi] \quad \text{(base joint unrestricted)} \\ & \theta_i \in [-\theta_{\text{lim}}, \theta_{\text{lim}}] \end{aligned} \tag{6}$$

B. Control Strategy

Once the known joint angle is established, the controller unlocks each joint, enabling them to move freely. The active actuator adjusts to the specified angle to set the corresponding joint. While the first joint can be easily positioned through subtraction, subsequent joints experience a shift in their center of mass due to the compounding weight and configuration. This shift must be taken into account. Figure 1 shows the example of a three-link system used to evaluate the repeatability of the system.

To find the torque for a system with k links,

$$\tau_i = g \sum_{n=i}^{k} m_n \left(\sum_{q=i}^{n-1} l_q \sin(\phi_q) + c_n \sin(\phi_n) \right) \tag{7}$$

where i is the link in consideration, m_n states the mass of nth link and $\phi_m = \sum_{j=1}^{m} \theta_j$.

Since the system is at rest, it can be considered to be in a state of static equilibrium. Thus, the torque can be set to 0.

$$\tau_i = 0 \tag{8}$$

Thus, by solving this, a generalized solution for the angle to be set for the second joint can be calculated as

$$\tan(\theta_1) = -\frac{\sum_{n=i}^{k} m_n \left(\sum_{p=i}^{n-1} l_p \sin(C_p) + c_n \sin(C_n) \right)}{\sum_{n=i}^{k} m_n \left(\sum_{p=i}^{n-1} l_p \cos(C_p) + c_n \cos(C_n) \right)} \tag{9}$$

where $C_n = \sum_{r=2}^{n} \theta_r$.

V. Evaluation

The goal of this evaluation is to assess the feasibility of a gravity-assisted shape-locking mechanism for use in ceiling-mounted robotic arms. The system is expected to move to specific locations with minimal error. This can prove that the actuation system is capable of positioning its end effector at the desired point. Furthermore, to understand the inherent errors within the system, a simple open-loop feed-forward actuation method was employed. This investigation aims to evaluate the robustness of the system, which will help determine the need for more complex feedback systems.

A. Hardware Setup

To evaluate the performance of the gravity-assisted shape-locking ceiling robot arm, we simplified the system by focusing on one active actuation unit and two passive joints. This approach not only simplifies the system but also reduces the workspace, allowing us to isolate key variables [32]. These changes also reduce the actuation dimensionality down to a planar workspace. As a result, we can conduct tests on fundamental mechanics by tracking with an RGB-D camera (Intel RealSense D455i), which enables a more straightforward analysis of system dynamics and control fidelity.

The passive 3D-printed joints remained free in all degrees of freedom, thus allowing their full range of motion and enabling the system to respond solely to gravitational and inertial forces. A silicone ball was affixed to the distal end of the assembly, serving dual roles as both a mass to induce gravitational actuation and a visual marker for motion tracking.

B. Software setup

The robot arm was set to move between two target points, while the position of the end effector was maintained. During the passage, the silicon ball target was tracked using the RGB-D camera. The camera is calibrated using a checkerboard method [33], and color masking was used to track the target object. To ensure the tracking accuracy, a region of interest and depth masking were used. Furthermore, five independent points were sampled and averaged when the robot arm was at rest. This allows for the removal of any vision and motion artifact, thus improving tracking consistency.

C. Analysis

The positional data was grouped into the targeted positions. The samples were grouped using the K-nearest neighbors algorithm. The groups were compared for means

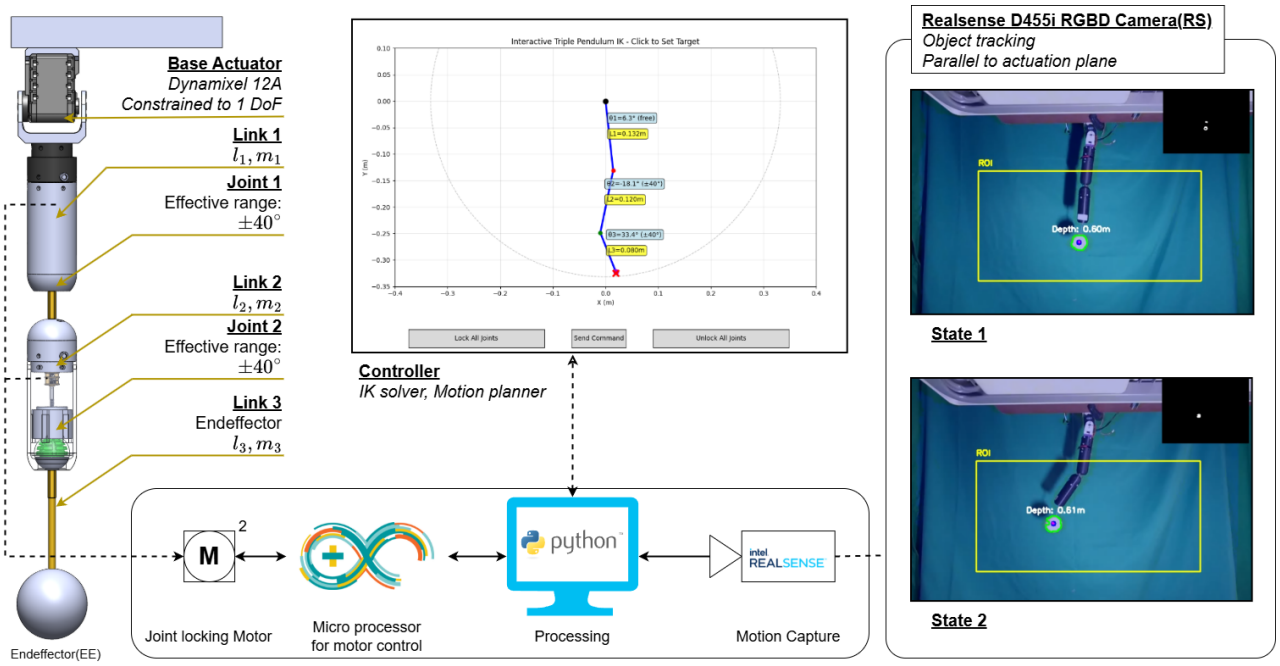

Parameter	Value [m]
$l_{RS\sim EE}$	0.65
$l_{[1,2,3]}$	$[0.13,\ 0.12,\ 0.08]$

Fig. 4. Overview of system validation hardware setup, software flow, and parameters used for IK controller.

and spread using the Kernel Density Estimate (KDE) and coefficient of variation (CV) for Cartesian repeatability on each axis. Furthermore, Principal Component Analysis(PCA) was conducted to see the trend. To further understand the clustering, the Silhouette score as well as the Dunn index were used to confirm the accuracy of the system.

The silhouette score and Dunn index are common internal validation metrics used to evaluate clustering quality, particularly in machine learning [34]. The silhouette score assesses how consistent data points are within a cluster by averaging the distance from each point to its nearest cluster neighbor and its farthest point in the cluster [35]. This score indicates the coherence of the motion. Similarly, the Dunn index compares the minimum and maximum separation between points within a cluster [36]. This provides a measure of how distinct the cluster is, as represented by the points the robot actuates.

D. Result

Figure 5 describes the collected position data after 300 cycles. The clustering is described in Table I. Group 1 and Group 2 denote the final end-effector positions after each reach. Each pair of points is clearly separated and exhibits meaningful clustering, demonstrating the accuracy of the evaluation system: The silhouette score for each group was 0.984 and 0.789, indicating the congruency of each group (~ 1.0). This is further observed from the Dunn index: 0.056 and 0.051. Dunn index with low and similar values indicates that the accuracy and repeatability are well understood.

Principal Component Analysis (PCA) reduces high-dimensional data by identifying the directions in which the most variation occurs. Using this, the shape of the cluster

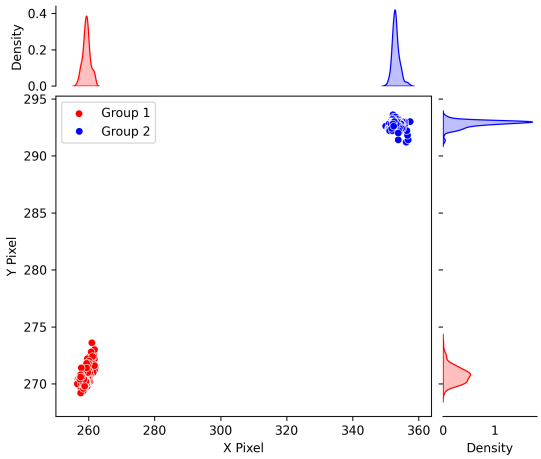

Fig. 5. The final pose of the end-effector corresponds to the instructed target configuration. KDE plots indicate the clustering of end position after 300 trials.

TABLE I

STATISTICAL ANALYSIS OF FINAL POSITION CLUSTERING TO TEST FEASIBILITY FOR CEILING ROBOT.

	SD [X, Y]	CV [X, Y] Pos. (%)	Silhouette (Dunn)
Group 1	$[1.15,\ 1.15]$	$[0.44,\ 0.33]$	0.984 (0.056)
Group 2	$[0.73,\ 0.35]$	$[0.27,\ 0.12]$	0.789 (0.051)

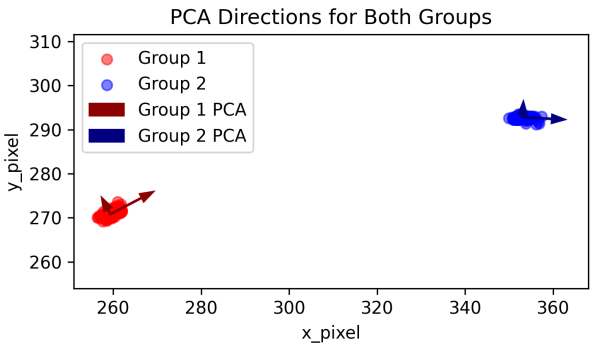

Fig. 6. PCA groups tested for repeatability. Group 1 VR=[0.866 0.133], Group 2 VR = [0.920 0.080]

can be further analyzed [32], [37]. Figure 6 entails the most significant principal component of the cluster, which shows the trend that is perpendicular to the rotation axis. This deviation can stem from residual vibration from the motor as well as the deflection from the system itself.

E. Discussion

The system evaluation confirmed that the actuation's repeatability and robustness achieved a silhouette score close to one (0.984, 0.789), making it well-suited for the intended accuracy. The capability to actuate the robot arm was confirmed through multiple trials, indicating consistent performance under controlled conditions. This can further suggest that with a gripper replacing a silicone ball as mass, the system has the capacity to perform a pick-and-place task, proving that the system is a viable solution for nursing-assistive robots.

One explanation for the bias observed in PCA is due to the small-angle problem(Figure 6). As the length of the robot arm increases, the small angle exerted by the actuation piece is expected to increase due to the long arm length. This issue is intrinsically embedded in the system. This problem is fixable by either segmenting the control points [38] or using a closed-loop system [39].

Alternatively, the accuracy of the system can benefit significantly from the implementation of a well-defined controller. The current open-loop configuration, while functional, lacks the dynamic adaptability required for high-precision tasks. An integration of a closed-loop control system would enhance the system's ability to respond to real-time feedback, thereby reducing positional errors and improving overall performance. Such improvements would not only increase accuracy but also contribute to more stable and reliable actuation over extended operational periods.

The robot arm relies on the material properties for load-bearing during passive mode. However, this cannot be replaced with strong materials like metals or increasing the friction force with a stronger motor because the current shape-locking mechanism depends heavily on withstanding the braking force generated by friction. Furthermore, the weights of each node compound, thus the mass exceeds the shape locking force. Various improvements may warrant increasing scalability.

Improving scalability can be achieved by enhancing the shape locking mechanism. Some researchers have reinforced the stiffness by Cross-Section Shaping [17], [18], increasing capacity by strengthening the structural integrity against the load. Many multi-material composites have been uncovered, including multi-layer jamming [19] and multi-layer beaming [20]. In this category, Jamming and Locking are included. In jamming, either longitudinal locking, such as a layer [21] or wire [22], can be used, or granular [23] can be used to strengthen the system. Polymer-based shape-locking and stiffness-variable actuators [40]–[42] were considered a possible improvement for soft robotics. These improvements can also speed up, as well as increase the load capacity.

This type of robot arm architecture exhibits the non-holonomic behavior. When moving from one setpoint to the other, the arm is not expected to follow a path. In extreme cases, the arm is set to reset to the default position. This action is most effective in conjunction with pick-and-place operations. However, further investigation is needed to assess the efficacy of this type of motion.

VI. Conclusion

In this paper, a novel gravity-assisted shape-locking ceiling robot was proposed as a possible expansion to the capabilities of current hospital ceiling lifts. This mechanism forms shapes by locking a passively driven secondary joint actuated from a primary joint. The shape-locking mechanism was utilized by using a small motor and friction pads, which constrained the motion of the ball joint linkages. Due to the active shape-locking mechanism on freely movable joints, the system can achieve both active and passive modes. The system was evaluated in reduced dimensions and reduced joints to validate its performance and robustness after repeated actuation. Although evaluated in a reduced prototype, the results suggest that ceiling-mounted systems can be extended beyond lifting alone to support pick-and-place and other assistive tasks. Future work will extend the prototype to 3D, integrate closed-loop control, and evaluate higher payloads.

References

[1] A. Baumann and M. Crea-Arsenio, "The crisis in the nursing labour market: Canadian policy perspectives," *Healthcare*, vol. 11, 2023. [Online]. Available: https://api.semanticscholar.org/CorpusID:259594384

[2] S. S. Birkhoff, P. Merring, A. Spence, W. Bassett, and S. C. Roth, "Integrating collaborative robots into a complex hospital setting: A qualitative descriptive study," *Delaware Journal of Public Health*, vol. 10, no. 5, p. 20, 2024.

[3] A. Dwivedi, "Medical robotic systems market revenue growth forecast by applications, regional analysis & industry players till 2032," Industry Market Report, 2025, accessed: 2025-09-15. [Online]. Available: https://philpapers.org/rec/DWIMRS

[4] G. L. Georgadarellis, T. Cobb, C. J. Vital, and F. C. Sup IV, "Nursing perceptions of robotic technology in healthcare: A pretest–posttest survey analysis using an educational video," *IISE Transactions on Occupational Ergonomics and Human Factors*, vol. 12, no. 1-2, pp. 68–83, 2024.

[5] J. Mayeda-Letourneau, "Safe patient handling and movement: a literature review," *Rehabilitation Nursing Journal*, vol. 39, no. 3, pp. 123–129, 2014.

[6] L. Bernhard, P. Schwingenschlögl, J. Hofmann, D. Wilhelm, and A. Knoll, "Boosting the hospital by integrating mobile robotic assistance systems: a comprehensive classification of the risks to be addressed," *Autonomous Robots*, vol. 48, no. 1, p. 1, 2024.

[7] D.-A. Brulotte, M. Faucher, and J. Bossé, "Configurable patient ceiling lift," Jan. 22 2019, uS Patent 10,182,955.

[8] H. Alamgir, O. W. Li, S. Yu, E. Gorman, C. Fast, and C. Kidd, "Evaluation of ceiling lifts: Transfer time, patient comfort and staff perceptions," *Injury*, vol. 40, no. 9, pp. 987–992, 2009. [Online]. Available: https://www.sciencedirect.com/science/article/pii/S0020138308005408

[9] K. Kozak, Q. Zhou, and J. Wang, "Static analysis of cable-driven manipulators with non-negligible cable mass," *IEEE Transactions on Robotics*, vol. 22, no. 3, pp. 425–433, 2006.

[10] I. D. Walker, "Continuous backbone "continuum" robot manipulators," *International Scholarly Research Notices*, vol. 2013, no. 1, p. 726506, 2013.

[11] S. Li and G. Hao, "Current trends and prospects in compliant continuum robots: a survey," in *Actuators*, vol. 10, no. 7. MDPI, 2021, p. 145.

[12] M. Manti, V. Cacucciolo, and M. Cianchetti, "Stiffening in soft robotics: A review of the state of the art," *IEEE Robotics & Automation Magazine*, vol. 23, no. 3, pp. 93–106, 2016.

[13] S. Hirose and M. Mori, "Biologically inspired snake-like robots," in *2004 IEEE International Conference on Robotics and Biomimetics*. ieee, 2004, pp. 1–7.

[14] K. McDonald, A. Rendos, S. Woodman, K. A. Brown, and T. Ranzani, "Magnetorheological fluid-based flow control for soft robots," *Advanced Intelligent Systems*, vol. 2, no. 11, p. 2000139, 2020.

[15] C. Pogue, P. Rao, Q. Peyron, J. Kim, J. Burgner-Kahrs, and E. Diller, "Multiple curvatures in a tendon-driven continuum robot using a novel magnetic locking mechanism," in *2022 IEEE/RSJ International Conference on Intelligent Robots and Systems (IROS)*. IEEE, 2022, pp. 472–479.

[16] I. D. Walker, D. M. Dawson, T. Flash, F. W. Grasso, R. T. Hanlon, B. Hochner, W. M. Kier, C. C. Pagano, C. D. Rahn, and Q. M. Zhang, "Continuum robot arms inspired by cephalopods," in *Unmanned Ground Vehicle Technology VII*, vol. 5804. SPIE, 2005, pp. 303–314.

[17] S. Kawamura, T. Yamamoto, D. Ishida, T. Ogata, Y. Nakayama, O. Tabata, and S. Sugiyama, "Development of passive elements with variable mechanical impedance for wearable robots," in *Proceedings 2002 IEEE International Conference on Robotics and Automation (Cat. No. 02CH37292)*, vol. 1. IEEE, 2002, pp. 248–253.

[18] O. Tabata, S. Konishi, P. Cusin, Y. Ito, F. Kawai, S. Hirai, and S. Kawamura, "Micro fabricated tunable bending stiffness devices," *Sensors and Actuators A: Physical*, vol. 89, no. 1-2, pp. 119–123, 2001.

[19] G. Mcknight, R. Doty, A. Keefe, G. Herrera, and C. Henry, "Segmented reinforcement variable stiffness materials for reconfigurable surfaces," *Journal of Intelligent Material Systems and Structures*, vol. 21, no. 17, pp. 1783–1793, 2010.

[20] L. Liu, X. Wang, Z. Wu, and T. Keller, "Resistance and ductility of frp composite hybrid joints," *Composite Structures*, vol. 255, p. 113001, 2021.

[21] S. Zuo, K. Iijima, T. Tokumiya, and K. Masamune, "Variable stiffness outer sheath with "dragon skin" structure and negative pneumatic shape-locking mechanism," *International journal of computer assisted radiology and surgery*, vol. 9, pp. 857–865, 2014.

[22] M. S. Moses, M. D. Kutzer, H. Ma, and M. Armand, "A continuum manipulator made of interlocking fibers," in *2013 IEEE International Conference on Robotics and Automation*. IEEE, 2013, pp. 4008–4015.

[23] J. R. Amend, E. Brown, N. Rodenberg, H. M. Jaeger, and H. Lipson, "A positive pressure universal gripper based on the jamming of granular material," *IEEE transactions on robotics*, vol. 28, no. 2, pp. 341–350, 2012.

[24] B. Yi, Y. Fan, and D. Liu, "A novel model for layer jamming-based continuum robots," in *2024 IEEE International Conference on Robotics and Automation (ICRA)*, 2024, pp. 12 727–12 733.

[25] L. Blanc, A. Delchambre, and P. Lambert, "Flexible medical devices: Review of controllable stiffness solutions," *Actuators*, vol. 6, p. 23, 2017. [Online]. Available: https://api.semanticscholar.org/CorpusID:31373209

[26] K. Kluszczyński and M. Kciuk, "Sma actuators: theory, performance curves and design problems," *COMPEL-The international journal for computation and mathematics in electrical and electronic engineering*, vol. 32, no. 4, pp. 1417–1427, 2013.

[27] E. M. McCabe, D. S. Esser, T. E. Ertop, A. Kuntz, and R. J. Webster III, "Combining thermoelectrics and low melting point alloys to create reconfigurable stiff-compliant manipulators," in *2024 IEEE 7th International Conference on Soft Robotics (RoboSoft)*. IEEE, 2024, pp. 711–715.

[28] T. McGeer *et al.*, "Passive dynamic walking," *Int. J. Robotics Res.*, vol. 9, no. 2, pp. 62–82, 1990.

[29] T. Yamawaki and M. Yashima, "Effect of gravity on manipulation performance of a robotic arm," in *Proceedings 2007 IEEE International Conference on Robotics and Automation*, 2007, pp. 4407–4413.

[30] J. Hu, T. Liu, H. Zeng, M. X. Chua, J. Katupitiya, and L. Wu, "Static modeling of a class of stiffness-adjustable snake-like robots with gravity compensation," *Robotica*, vol. 12, p. 2, 2022.

[31] V. Arakelian, "Gravity compensation in robotics," *Advanced robotics*, vol. 30, no. 2, pp. 79–96, 2016.

[32] I. K. Fodor *et al.*, "A survey of dimension reduction techniques," *Technical Report UCRL-ID-148494, Lawrence Livermore National Laboratory*, 2002.

[33] C. Tomasi and T. Kanade, "Detection and tracking of point," *Int J Comput Vis*, vol. 9, no. 137-154, p. 3, 1991.

[34] G. Blasilli, D. Kerrigan, E. Bertini, and G. Santucci, "Towards a Visual Perception-Based Analysis of Clustering Quality Metrics," in *2024 IEEE Visualization in Data Science (VDS)*, Oct. 2024, pp. 15–24. [Online]. Available: https://ieeexplore.ieee.org/document/10747684

[35] P. J. Rousseeuw, "Silhouettes: A graphical aid to the interpretation and validation of cluster analysis," *Journal of Computational and Applied Mathematics*, vol. 20, pp. 53–65, Nov. 1987. [Online]. Available: https://www.sciencedirect.com/science/article/pii/0377042787901257

[36] J. C. Dunn, "A Fuzzy Relative of the ISODATA Process and Its Use in Detecting Compact Well-Separated Clusters," *Journal of Cybernetics*, vol. 3, no. 3, pp. 32–57, Jan. 1973. [Online]. Available: https://doi.org/10.1080/01969727308546046

[37] C. Ding and X. He, "K-means clustering via principal component analysis," in *Proceedings of the twenty-first international conference on Machine learning*, 2004, p. 29.

[38] A. Doroudchi, S. Shivakumar, R. E. Fisher, H. Marvi, D. Aukes, X. He, S. Berman, and M. M. Peet, "Decentralized control of distributed actuation in a segmented soft robot arm," in *2018 IEEE Conference on Decision and Control (CDC)*. IEEE, 2018, pp. 7002–7009.

[39] A. Doroudchi, Z. Qiao, W. Zhang, and S. Berman, "Configuration tracking control of a multi-segment soft robotic arm using a cosserat rod model," *arXiv preprint arXiv:2210.00182*, 2022.

[40] H. M. Le, P. T. Phan, C. Lin, L. Jiajun, and S. J. Phee, "A temperature-dependent, variable-stiffness endoscopic robotic manipulator with active heating and cooling," *Annals of Biomedical Engineering*, vol. 48, no. 6, p. 1837–1849, Jun. 2020.

[41] Y. Yang, Y. Chen, Y. Li, and M. Z. Chen, "3d printing of variable stiffness hyper-redundant robotic arm," in *2016 IEEE International Conference on Robotics and Automation (ICRA)*. IEEE, 2016, pp. 3871–3877.

[42] N. G. Cheng, A. Gopinath, L. Wang, K. Iagnemma, and A. E. Hosoi, "Thermally tunable, self-healing composites for soft robotic applications," *Macromolecular Materials and Engineering*, vol. 299, no. 11, pp. 1279–1284, 2014.